Heavy-residue production in Ar-Th collisions at 44, 77, and 95 MeV/nucleon

R. Yanez,[1] W. Loveland,[2] K. Aleklett,[1] A. Srivastava,[2] and J.O. Liljenzin[3]
[1]*Studsvik Neutron Research Laboratory, S-611 82 Nyköping, Sweden*
[2]*Department of Chemistry, Oregon State University, Corvallis, Oregon 97331*
[3]*Chalmers University of Technology, Göteborg, Sweden*
(Received 14 October 1994)

The yields and recoil properties of the targetlike fragments produced in the interaction of 44, 77, and 95 MeV/nucleon Ar with ^{232}Th have been measured. From these data, the fragment mass distributions, average energies, and the linear momentum transfer leading to their formation have been deduced. The residue yields are large at all energies [790 mb, 790 mb, and 710 mb (±30%) at 44, 77, and 95 MeV/nucleon, respectively] while the average residue energies are low [mean fractional linear momentum transfer (FLMT) is 0.14, 0.12, and 0.13 for the 44, 77, and 95 MeV/nucleon experiments]. Because of the low mean FLMT values associated with the residues, we conclude that, on average, they do not result from fusionlike events. The residue energies and their dependence on fragment mass number agree with predictions of BUU calculations. The substantial survival of the residues of excited, fissionable nuclei is shown to be a result of retardation of fission decay and the broad primary fragment distributions. The intranuclear cascade model is shown to give an incorrect description of the primary fragment properties in these reactions.

PACS number(s): 25.70.Mn, 27.90.+b

I. INTRODUCTION

A central theme in the study of intermediate energy nuclear collisions ($10 \leq E_{\rm proj} \leq 200$ MeV/nucleon) is the evolution of reaction mechanisms with increasing projectile energy. At the lowest energies, the effect of the nuclear mean field is dominant as evidenced in the complete fusion reaction mechanism. As the relative velocity of the colliding nuclei increases, collisions between individual nucleons become more important and the effect of the nuclear mean field becomes less important. This change is mirrored in the increasing importance of incomplete fusion and spallationlike phenomena.

The Ar+Th reaction has played an important role in our understanding of intermediate energy nuclear collisions. Measurements [1,2] of the fission fragment folding angle distributions for this reaction showed the disappearance of fusionlike events at a projectile energy of 39–44 MeV/nucleon. Originally this disappearance was linked to the idea of the maximum excitation energy that could be contained in a nucleus, but similar studies [3] of the Ni + Th reaction showed the persistence of fusionlike events up to $E^* \sim 900$ MeV, a value greater than that achieved in the Ar+Th reaction. Measurement [4,5] of the neutron multiplicities for the Ar+Th reaction showed a constant average multiplicity while the Ar energy varied from 27 to 77 MeV/nucleon and the occurrence of similar multiplicity distributions. So clearly large multiplicity (large momentum transfer, fusionlike) events were occurring at projectile energies above 40 MeV/nucleon although they were absent from the folding angle distributions.

Two possible reaction exit channels in which one might find the "missing" fusionlike events were the heavy residues and true multifragmentation events that do not leave a heavy target residue. [The frequently used term "intermediate mass fragments" can include lower Z (Z =1–5) fragments whose production also includes that of a heavy targetlike fragment.] Independent evidence was found [6–9] that the time scale of fission events for the Ar+Th system was $\sim 10^{-20}$ sec, which is long compared to the time for neutron emission of $\sim 10^{-22}$ sec. Thus, fission was expected to be severely inhibited for $E^* > 50 - 75$ MeV.

Recently, Utley *et al.* [10] identified the formation of heavy evaporation residues resulting from central collisions in the interaction of 40 MeV/nucleon ^{40}Ar with ^{232}Th. From associated neutron multiplicities, they could associate excitation energies of 880±120 MeV with these products, consistent with their formation in fusionlike events. The actual observed multiplicities in this work were much higher than those observed previously [4,5] presumably because they were associated only with the highest momentum transfer events and not averaged over a range of impact parameters and momentum transfers. Comparison of their results to reaction simulations allowed Utley *et al.* to conclude that a dynamic delay of $1–5\times10^{-20}$ s in the fission channel was occurring. The results of Utley *et al.* are consistent with the findings [11] in a lighter system, Ar+Ag, at projectile energies of 50–70 MeV/nucleon of evidence for the formation of heavy residues with high excitation energies ($\sim$ 600 MeV).

Pollacco *et al.* [12] have also reported finding massive fragments from the ^{40}Ar+^{232}Th reaction at 44 and 77 MeV/nucleon that were the result of events involving high excitation energies. They found heavy fragment production cross sections for these events that were small (200–300 mb) although it should be noted that their detection thresholds were 0.5 cm/ns, a value shown [13] to cause one to miss most targetlike fragments. They attribute these fragments to deep inelastic processes, in part.

Despite these observations of evaporation residues from fusionlike events, there remains the issue of quantitatively accounting for how the Ar+Th reaction cross section is divided among the various reaction exit channels as the projectile energy increases. We thought it would be useful to measure, using radiochemical techniques, the gross cross sections for heavy residue and intermediate mass fragment production, and their momenta for the Ar+Th reaction at energies (44, 77, and 95 MeV/nucleon) where the fusionlike events were absent from the folding angle distributions, but present in the neutron multiplicities. The use of radiochemical techniques to study the heavy residue properties was to ensure that no residues would be missed due to detection thresholds, etc. [13]. The choice of a very fissile system with higher projectile energies is to allow us to investigate further the nature of particle-evaporation/fission competition at high excitation energies.

We present the results of that investigation in this paper. We find substantial yields of the heavy residues even with a target nucleus as fissionable as ^{232}Th. However, the magnitude of the observed residue cross section and its association with low momentum transfer events indicates that the heavy residues are not responsible for all of the "missing" fusionlike events. We consider, in some detail using the BUU model, how these residues could have been formed.

In Sec. II of this paper we discuss the experimental arrangements and details of the measurements. The results of these measurements, the residue yields, energies, and the momentum transfers leading to their formation are discussed in Sec. III. A discussion of these results and the general question of the survival of fissionable targetlike fragments is given in Sec. IV. Conclusions are presented in Sec. V.

II. EXPERIMENTAL

These radiochemical experiments were carried out at the GANIL laboratory (Grand Accélerateur National d'Ions Lourdes) at Caen, France. In the experiment with 44 MeV/nucleon ^{40}Ar, a thin thorium metal target (0.9 mg/cm^2) was sandwiched between two carbon catcher foils of thickness 14.5 mg/cm^2 (backward) and 32 mg/cm^2 (forward). This foil stack was irradiated with 44 MeV/nucleon ^{40}Ar projectiles with 3.0×10^{14} ions passing through the target in 30 min. The center-of-target energy of the beam was 42.6 MeV/nucleon [14]. In the higher energy experiments, thick targets of thorium metal (55.94 mg/cm^2) were surrounded by 17.5 mg/cm^2 Mylar catcher foils (Fig. 1). These targets were irradiated by 77 MeV/nucleon ^{40}Ar and 95 MeV/nucleon ^{36}Ar ions in separate experiments. (At 95 MeV/nucleon, two separate irradiations of duration 7 and 64 min. were performed to enhance detection of the shortest-lived nuclides. At 77 MeV/nucleon, a single irradiation lasting 19.3 min. was made. The particle fluences for the three irradiations were 2.9×10^{13}, 2.5×10^{14}, and 7.3×10^{13}, respectively.) The center-of-target beam energies are 76.1 and 94.1 MeV/nucleon [14]. Since the projectile energy loss in the target is small and to facilitate comparison with other work, we shall refer to the incident projectile energies in describing our measurements. The radionuclide content of the target, forward and backward catcher foils, was determined by off-line gamma-ray spectroscopy. Production cross sections were calculated from end of bombardment activities [15]. Typically we observed 2–3 gamma lines per nuclide with the range being 1 to 11.

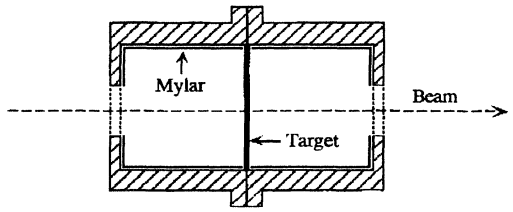

FIG. 1. Schematic diagram of the apparatus to study the interaction of 77 and 95 MeV/nucleon Ar with ^{232}Th.

As indicated in Fig. 1, in the two higher energy experiments, small ($\sim$ 10 mm diam.) holes were drilled in both the forward and backward Mylar catcher foils to prevent radiation damage of the Mylar by the beam. The forward and backward foil activities were corrected for recoils escaping through these holes by appropriate integrations of the fragment angular distributions from the 93 MeV/nucleon ^{36}Ar+^{197}Au reaction [16] and assuming the Ar-Th and Ar-Au residue distributions to be similar. The magnitude of the corrections was $\sim$1–6 %. A numerical simulation using the LINDA code [17] showed that 26 and 25 % of the full momentum transfer events would be missed at projectile energies of 77 and 95 MeV/nucleon, respectively. (Most residues stop in the thick target.) Assuming the more reasonable scenario [10] of a maximum linear momentum transfer of 180 MeV/c per projectile nucleon, the number of missed fusionlike events in the cross section measurements is 11 and 8 % at 77 and 95 MeV/nucleon, respectively. In measurements of the recoil properties of the fusionlike events, $\sim$50% of them would have been detected. Thus, evaporation residues originating from fusionlike events should be present in our higher energy data although there is a modest bias against such events. No such corrections are needed for the 44 MeV/nucleon experiment.

III. RESULTS

The nuclidic production cross sections for the 124 different radionuclides formed in the interaction of 44 MeV/nucleon ^{40}Ar with ^{232}Th are listed in Table I. Tables II and III contain similar listings for the 176 and 151 different radionuclides found from the interaction of 77 MeV/nucleon ^{40}Ar and 95 MeV/nucleon ^{36}Ar with ^{232}Th. Also shown in these tables are the thick target-thick catcher recoil properties, F/B and $2W(F+B)$. F/B is the ratio of products recoiling into the forward (F) and backward (B) catcher foils while $2W(F+B)$ represents the fraction of all nuclides recoiling out of the target, $F+B$, multiplied by twice the target thickness

TABLE I. Nuclide yields and recoil properties for the interaction of 44 MeV/nucleon ^{40}Ar with ^{232}Th.

Nucleus[a]	Cross section[b]	F/B	$2W(F+B)$[c]	Nuclide	Cross section [b]	F/B	$2W(F+B)$[c]
^{24}Na	59.1± 0.7	5.3± 0.1	1.25± 0.02	^{129}Cs	30.9± 0.5	3.18± 0.38	1.61± 0.11
^{28}Mg	12.4± 0.9	7.5± 0.4	1.75± 0.04	^{131}I	14.1± 0.5	1.21± 0.07	1.69± 0.05
^{42}K	12.7± 0.9	-	-	^{132}Te	7.4± 1.7	1.34± 0.08	1.67± 0.05
^{43}K	14.4± 0.7	3.8± 0.4	1.72± 0.09	^{132}La*	10.5± 0.6	4.50± 0.58	1.60± 0.09
^{44}Sc	1.9± 0.2	-	-	^{132}Ce	14.0± 0.4	4.62± 0.25	1.63± 0.06
^{44}Sc^{m*}	3.9± 1.1	-	-	^{132}Cs	14.0± 0.4	-	-
^{47}Ca	4.0± 0.2	-	-	^{133}I	11.5± 0.3	1.05± 0.05	1.71± 0.04
^{48}Sc	7.9± 0.7	2.6± 0.1	1.65± 0.04	^{135}I	8.5± 0.4	-	-
^{52}Mn	5.5± 0.3	1.19± 0.15	0.59± 0.04	^{135}Xe	11.2± 0.7	-	-
^{56}Mn	60.3± 4.2	2.4± 0.1	0.54± 0.01	^{135}Ce	19.8 ± 2.8	4.00± 0.25	1.62± 0.04
^{71}As	4.4± 0.1	2.7± 0.1	1.73± 0.04	^{138}Pr^{m}	4.4± 0.4	2.47± 0.50	1.65± 0.16
^{72}Zn	4.6± 0.2	1.24± 0.10	1.66± 0.07	^{139}Ba	13.9± 2.1	-	-
^{76}As	19.5± 0.6	-	-	^{140}Ba	12.1± 0.6	1.17± 0.08	1.70± 0.06
^{77}Br	13.3± 0.2	-	-	^{142}La	13.1± 1.0	-	-
^{78}As	16.5± 0.3	-	-	^{143}Ce	10.3± 0.4	1.13± 0.06	1.71± 0.04
^{79}Kr	13.7± 0.7	2.46± 0.27	1.59± 0.09	^{145}Eu	7.6± 0.1	-	-
^{81}Rb*	8.4± 0.8	2.17± 0.21	1.74± 0.09	^{147}Gd	11.0± 0.8	6.77± 0.70	1.50± 0.06
^{82}Br*	13.5± 0.4	1.63± 0.12	1.71± 0.06	^{149}Gd	18.0± 0.8	5.53± 1.17	1.63± 0.11
^{82}Rb^{m*}	10.2± 0.8	2.24± 0.27	1.70± 0.10	^{151} Tb	8.6± 1.0	-	-
^{83}Sr	6.9± 1.0	2.22± 0.31	1.54± 0.11	^{152}Tb	12.0± 1.4	8.9± 1.8	1.53± 0.24
^{85}Kr^{m*}	17.2± 0.3	1.07± 0.05	1.71± 0.04	^{153} Tb	14.6± 0.4	7.36± 0.38	1.56± 0.05
^{86}Y	10.6± 0.3	2.62± 0.10	1.70± 0.03	^{155}Tb	17.9± 1.1	-	-
^{86}Zr	8.0± 0.7	2.90± 0.39	1.64± 0.14	^{155}Dy	13.5± 0.4	14.2± 1.0	1.55± 0.04
^{87}Y	24.7± 0.8	2.36± 0.11	1.70± 0.04	^{157}Dy	16.6± 0.4	8.0± 0.3	1.56± 0.04
^{87}Y^{m}	22.4± 0.5	2.45± 0.09	1.67± 0.03	^{158}Er	12.1± 0.7	-	-
^{88}Kr	12.9± 1.8	-	-	^{160}Er	11.1± 0.4	-	-
^{89}Zr	20.5± 0.4	2.23± 0.08	1.70± 0.03	^{161}Er	14.0± 1.3	-	-
^{90}Y^{m*}	20.4± 2.1	1.59± 0.11	1.68± 0.05	^{165} Tm	11.8± 1.1	-	-
^{90}Nb	8.2± 0.2	-	-	^{166}Yb	21.2± 1.5	2.48± 0.09	1.65± 0.03
^{91}Sr	38.4± 2.8	1.24± 0.06	1.71± 0.05	^{167}Tm	14.1± 0.5	-	-
^{92}Sr	23.3± 0.6	1.02± 0.05	1.70± 0.04	^{169}Lu	9.3± 0.4	-	-
^{92}Y	54.5± 2.8	1.15± 0.10	1.70± 0.07	^{170}Hf	8.6 ± 0.1	-	-
^{93}Y	54.8± 5.5	1.75± 0.29	1.67± 0.15	^{171}Hf	10.6± 0.5	-	-
^{95}Tc	10.5± 1.0	2.47± 0.45	1.66± 0.19	^{173}Hf	13.0± 1.5	15.0± 0.7	1.46± 0.07
^{96}Nb	18.2± 0.7	1.65± 0.12	1.72± 0.07	^{173}Ta	21.0± 2.4	1.67± 0.36	1.68± 0.21
^{96}Tc	12.1± 0.2	2.51± 0.33	1.66± 0.10	^{174}Ta	12.9± 1.0	-	-
^{97}Zr	29.2± 1.0	1.21± 0.04	1.71± 0.03	^{175}Ta	8.4± 1.1	-	-
^{97}Nb	16.7± 2.4	-	-	^{176}Ta	9.6± 0.8	-	-
^{97}Ru	11.9± 0.3	2.98± 0.13	1.65± 0.03	^{177}W	5.0 ± 0.4	-	-
^{99}Mo	54.8± 0.5	1.21± 0.10	1.70± 0.07	^{181}Re	7.1± 0.4	-	-
^{100}Rh	10.4± 0.2	-	-	^{182}Os	6.4± 0.6	-	-
^{101}Rh^{m*}	20.9± 1.1	2.22± 0.22	1.68± 0.09	^{184}Ir	1.2± 0.2	-	-
^{105}Ru	50.1± 1.5	1.19± 0.06	1.71± 0.04	^{192}Au	2.3± 0.2	-	-
^{110}In^{m*}	8.3± 1.3	2.69± 0.19	1.58± 0.06	^{192} Hg	3.8± 0.3	-	-
^{111}In	18.3± 0.3	2.96± 0.13	1.67± 0.04	^{199}Pb	1.9± 0.3	-	-
^{115}Cd*	29.1± 0.8	1.15± 0.05	1.71± 0.04	^{200}Tl	2.8± 0.6	-	-
^{117}Cd	6.8± 0.6	-	-	^{200}Pb	3.0± 0.3	-	-
^{117}Cd^{m}	22.3± 0.8	1.27± 0.07	1.72± 0.05	^{201}Tl	5.1± 0.8	-	-
^{117}Te	8.2± 0.8	-	-	^{201}Pb	3.2± 0.1	-	-
^{118}Sb^{m*}	9.7± 0.3	2.14± 0.12	1.71± 0.05	^{202} Bi	3.5± 0.3	-	-
^{119}Te^{m*}	8.9± 0.3	2.97± 0.15	1.60± 0.04	^{203} Pb	4.3± 0.1	-	-
^{119}Te	10.1± 0.3	3.76± 0.21	1.68± 0.05	^{203}Bi	2.3± 0.1	-	-
^{120}Sb*	10.4± 1.5	1.86± 0.10	1.70± 0.04	^{204}Bi	3.5± 0.1	-	-
^{121}I	17.6± 0.8	2.63± 0.23	1.62± 0.08	^{205}Bi	6.8± 1.6	-	-
^{122}Sb	13.8± 0.4	1.54± 0.08	1.68± 0.04	^{205}Po	2.0± 0.1	-	-
^{123}Xe	12.5± 0.7	2.77± 0.42	1.65± 0.09	^{206}Bi	6.0± 0.7	-	-
^{124}I	12.2± 0.3	1.80± 0.08	1.69± 0.04	^{206}Po	4.9± 0.1	-	-
^{125}Xe	21.9± 0.6	3.27± 0.15	1.63± 0.04	^{207}Po	4.2± 0.2	-	-
^{127}Sb	10.2± 1.3	1.21± 0.12	1.66± 0.09	^{209}At	5.1± 0.1	-	-
^{127}Xe	24.7± 2.8	2.60± 0.31	1.67± 0.11	^{210}At	3.5± 0.3	-	-

TABLE I. (*Continued*).

Nucleus[a]	Cross section[b]	F/B	$2W(F+B)$[c]	Nuclide	Cross section[b]	F/B	$2W(F+B)$[c]
^{127}Cs	23.4± 2.1	3.97± 0.24	1.47± 0.04	^{211}Rn	2.4± 0.2	-	-
^{128}Ba	15.9± 0.6	4.43± 0.47	1.62± 0.07				
^{129}Sb	3.9± 0.5	-	-				

[a]The asterisk denotes a nuclide not used in computation of isobaric yields due to unknown yield of other members of isomeric pair.
[b]In mb.
[c]In mg/cm^2 Th.

TABLE II. Nuclide yields and recoil properties for the interaction of 77 MeV/nucleon ^{40}Ar with ^{232}Th.

Nucleus[a]	Cross section[b]	F/B	$2W(F+B)$[c]	Nuclide	Cross section[b]	F/B	$2W(F+B)$[c]
^{24}Na	34.1± 0.1	27.3± 0.4	43.1± 0.2	^{125}Xe	14.2± 0.1	3.5± 0.1	3.6± 0.1
^{28}Mg	11.2± 0.6	27.7± 0.9	40.6± 0.4	^{126}Sb*	5.3 ± 0.1	1.43± 0.06	8.0± 0.2
^{38}S	2.3± 0.1	-	-	^{126}I	7.2± 0.4	2.7± 0.4	7.2± 0.5
^{42}K	9.6± 0.1	14.2± 1.3	25.0± 0.6	^{126}Ba	8.1± 0.4	-	-
^{43}K	10.5± 0.1	10.3± 0.4	20.6± 0.4	^{127}Sb	6.7± 0.1	1.62± 0.13	7.9± 0.3
^{44}Sc^m	3.4± 1.2	16.4± 0.9	15.7± 0.3	^{127}Xe	18.2± 0.7	-	-
^{44}Sc	0.8± 0.1	-	-	^{127}Cs	18.8± 0.3	8.4± 0.5	5.1± 0.1
^{46}Sc	10.6± 0.2	18± 0.7	20.0± 0.3	^{128}Sb*	2.6± 0.1	1.59± 0.17	7.5± 0.4
^{47}Ca	3.4± 0.1	5.9± 0.6	15.0± 0.6	^{128}Ba	10.2± 0.1	4.2± 0.4	6.4± 0.3
^{48}Sc	6.4± 0.3	8.7± 0.3	16.2± 0.2	^{129}Sb	2.5± 0.2	1.75± 0.28	10.8± 0.9
^{48}V	2.1± 0.1	16.3± 3.6	17.8± 0.6	^{129}Cs	21.1± 0.2	5.7± 0.3	6.5±0.2
^{56}Mn	9.4± 0.2	6.2± 0.8	13.4± 0.5	^{130}I*	5.2± 0.1	1.49± 0.05	7.8± 0.1
^{58}Co	6.0± 0.1	10.6± 2.2	13.3± 0.5	^{131}Te^{m*}	6.3± 0.2	1.52± 0.23	7.1± 0.6
^{59}Fe	8.8± 0.1	4.0± 0.2	12.5± 0.3	^{131}I	12.6± 0.1	1.34± 0.02	8.0± 0.1
^{69}Zn^{m*}	7.1± 0.1	2.77± 0.05	11.4± 0.1	^{131}Ba	13.9± 1.5	7.4± 0.4	7.0± 0.1
^{71}Zn^{m*}	3.1± 0.3	1.93± 0.10	10.9± 0.3	^{132}Te	5.7± 0.8	1.25± 0.05	7.4± 0.2
^{71}As	3.3± 0.1	6.3± 0.2	12.7± 0.2	^{132}I*	3.2± 0.2	1.33± 0.18	11.2± 0.8
^{74}As	11.2± 0.1	3.5± 0.1	10.2± 0.2	^{132}Cs	6.4± 0.2	-	-
^{75}Se	9.5± 0.1	4.4± 0.3	10.7± 0.2	^{132}La*	8.4± 0.3	14.8± 2.3	5.9± 0.2
^{75}Br	0.7± 0.1	-	-	^{132}Ce	10.1± 0.2	14.0± 0.7	6.5± 0.2
^{76}As	12.2± 0.5	2.8± 0.3	9.5± 0.5	^{133}I	10.2± 0.1	1.30± 0.03	8.2± 0.1
^{76}Br	3.0± 0.2	-	-	^{135}I	7.8± 0.1	1.62± 0.13	8.5± 0.3
^{77}Ge*	4.7± 0.2	1.20± 0.10	8.6± 0.4	^{135}Xe	10.7 ± 0.1	-	-
^{77}Br	10.2± 0.1	3.8± 0.2	9.3± 0.3	^{135}Ce	12.5± 0.4	8.9± 1.1	5.7± 0.1
^{78}As	11.5± 0.8	1.31± 0.08	13.2± 0.4	^{136}Cs*	3.1± 0.1	1.49± 0.08	7.6± 0.2
^{79}Kr	11.4± 0.4	-	-	^{139}Ba	12.3± 0.3	-	-
^{81}Rb*	6.0± 0.1	5.0± 0.2	10.6± 0.2	^{139}Ce	14.9± 0.3	-	-
^{82}Br*	11.0± 0.1	1.89± 0.10	9.6± 0.3	^{140}Ba	9.9 ± 0.1	1.24± 0.05	7.3± 0.1
^{82}Rb^{m*}	9.7± 0.2	4.2± 0.4	8.2± 0.3	^{141}Ce	14.1± 0.3	1.53± 0.07	6.1± 0.2
^{83}Rb	18.8± 0.4	3.5± 0.2	9.3± 0.3	^{142}La	9.7± 0.1	1.87± 0.15	9.9± 0.4
^{83}Sr	5.4± 0.1	4.2± 0.4	8.4± 0.4	^{143}Ce	8.4± 0.1	-	-
^{84}Rb	15.8± 1.4	2.9± 0.4	9.3± 0.7	^{145}Eu	9.2± 1.4	-	-
^{85}Y^{m*}	4.9± 0.1	4.1± 0.3	9.8± 0.4	^{146}Gd	9.8± 0.1	-	-
^{86}Rb*	23.2± 0.4	3.1± 0.3	7.5± 0.3	^{147}Eu	13.3± 2.8	-	-
^{86}Y	9.1± 0.2	4.4± 0.1	8.2± 0.1	^{147}Gd	9.5± 0.6	4.6± 0.4	5.4± 0.2
^{87}Kr	16.2± 0.2	-	-	^{148}Eu	2.1± 0.1	-	-
^{87}Y	19.6± 0.1	4.5± 0.1	8.3± 0.1	^{149}Gd	12.9± 0.1	-	-
^{87}Y^m	15.5± 0.6	3.8± 0.2	8.3± 0.3	^{151}Tb	8.3 ± 0.8	-	-
^{88}Y	16.0± 0.4	3.1± 0.1	8.9± 0.2	^{152}Dy	6.4± 0.2	-	-
^{88}Zr	12.2± 0.3	5.2± 0.3	8.0± 0.3	^{153}Tb	9.8± 0.2	-	-
^{89}Zr	15.3± 0.1	4.3± 0.2	8.2± 0.1	^{155}Dy	7.6± 0.2	-	-
^{90}Y^{m*}	14.3± 0.1	2.22± 0.05	9.4± 0.1	^{157}Dy	11.9± 0.1	9.0± 0.3	5.2± 0.1
^{90}Nb	7.2± 0.1	5.3± 0.2	8.5± 0.2	^{158}Er	9.1± 0.1	-	-
^{91}Sr	27.4± 0.4	1.33± 0.04	10.7± 0.2	^{160}Er	10.7± 0.7	-	-
^{92}Sr	20.7± 0.1	1.24± 0.03	10.2± 0.1	^{161}Er	11.3± 0.3	-	-

TABLE II. (*Continued*).

Nucleus[a]	Cross section[b]	F/B	$2W(F+B)$[c]	Nuclide	Cross section[b]	F/B	$2W(F+B)$[c]
^{92}Y	28.6± 0.6	1.17± 0.08	8.7± 0.3	^{165}Tm	10.2± 0.9	-	-
^{93}Y	39.6± 1.1	1.40± 0.09	7.5± 0.2	^{166}Yb	8.4± 0.6	-	-
^{93}Mo^{m*}	5.1± 0.1	5.1± 0.3	7.9± 0.2	^{167}Tm	10.5± 0.1	-	-
^{94}Tc*	3.5± 0.1	3.5± 0.3	7.1± 0.3	^{169}Yb	10.6± 1.5	-	-
^{95}Zr	40.0± 1.4	1.39± 0.04	8.5± 0.1	^{169}Lu	9.8± 0.4	-	-
^{95}Nb	22.2± 1.4	-	-	^{170}Hf	8.5± 1.5	-	-
^{95}Ru	2.7± 0.4	-	-	^{171}Lu	10.6± 0.1	-	-
^{96}Nb	16.1± 0.5	1.97± 0.04	8.9± 0.1	^{171}Hf	8.8± 0.3	-	-
^{96}Tc	8.5± 0.1	4.0± 0.2	7.7± 0.2	^{173}Hf	9.7± 0.3	-	-
^{97}Zr	24.4± 0.2	1.36± 0.03	10.3± 0.1	^{173}Ta	18.3± 0.7	-	-
^{97}Nb	15.7± 0.5	2.11± 0.23	8.9± 0.4	^{175}Hf	4.0± 0.6	-	-
^{97}Ru	8.9± 0.1	6.8± 0.4	7.2± 0.2	^{176}Ta	11.5± 0.1	-	-
^{99}Mo	46.4± 0.6	1.70± 0.05	10.4± 0.2	^{177}W	5.4± 0.1	-	-
^{99}Rh^{m*}	3.7± 0.1	6.3± 0.5	8.9± 0.3	^{181}Re	7.3± 0.1	-	-
^{100}Rh	8.1± 1.3	6.1± 0.3	6.7± 0.1	^{182}Os	7.4± 0.1	-	-
^{101}Rh^{m*}	12.5± 0.1	4.7± 0.1	7.7± 0.1	^{183}Re	5.5± 0.4	-	-
^{103}Ru	61.0± 1.4	1.55± 0.09	-	^{184}Ir	5.3± 0.1	-	-
^{105}Ru	44.2± 0.4	1.38± 0.03	9.7± 0.1	^{185}Os	8.5 ± 0.2	-	-
^{105}Rh	56.8± 0.8	1.68± 0.06	9.8± 0.7	^{185}Ir	4.0 ± 0.1	-	-
^{105}Ag	8.5± 0.7	-	-	^{186}Pt	3.8± 0.1	-	-
^{106}Rh^{m*}	13.9± 0.4	2.06± 0.17	8.3± 0.4	^{188} Pt	5.0± 0.6	-	-
^{106}Ag^{m*}	7.1± 0.1	3.2± 0.3	9.4± 0.4	^{192}Au	3.5± 0.2	-	-
^{110}Ag^{m*}	11.9± 0.1	2.03± 0.19	7.7± 0.4	^{192} Hg	5.7± 0.1	-	-
^{110}In*	5.9± 0.1	6.7± 0.8	6.9± 0.3	^{199}Pb	7.4± 0.3	-	-
^{111}In	12.6± 0.2	5.1± 0.2	7.5± 0.1	^{200}Tl	4.4± 0.1	-	-
^{113}Ag*	40.3± 0.8	1.49± 0.10	10.3± 0.4	^{200}Pb	3.9± 0.1	-	-
^{115}Cd*	25.7± 0.4	1.41± 0.04	8.8± 0.1	^{201}Pb	5.3± 0.1	-	-
^{116}Te	6.1± 0.8	-	-	^{202}Tl	5.1± 0.1	-	-
^{117}Cd	6.7± 0.2	1.46± 0.11	10.0± 0.4	^{202}Bi	4.4 ± 0.5	-	-
^{117}Cd^{m}	18.3± 1.5	1.40± 0.04	8.7± 0.1	^{203}Pb	7.3± 0.1	-	-
^{117}Te	8.4± 0.3	-	-	^{203}Bi	3.6± 0.1	-	-
^{118}Sb^{m*}	7.4± 0.3	3.4± 0.2	7.5± 0.3	^{204}Bi	6.7± 0.1	-	-
^{119}Te	7.8± 0.1	8.8± 0.5	6.5± 0.1	^{204}Po	7.5± 0.6	-	-
^{119}Te^{m}	5.9± 0.3	4.7± 0.3	7.3± 0.2	^{205}Bi	6.8± 0.8	-	-
^{120}Sb*	7.2± 0.1	2.5± 0.1	8.3± 0.2	^{205}Po	4.7± 0.3	-	-
^{120}I*	10.8± 0.2	4.3± 0.4	6.2± 0.2	^{206}Bi	9.4± 0.1	-	-
^{121}Te	11.1± 0.4	4.9± 0.4	6.8± 0.4	^{206}Po	9.6± 0.2	-	-
^{121}Te^{m}	5.7± 0.8	-	-	^{207}Po	4.3± 0.1	-	-
^{121}I	11.3± 0.3	6.4± 0.4	6.9± 0.2	^{207}At	7.3± 0.1	-	-
^{122}Sb	9.5± 0.1	1.9± 0.1	7.6± 0.2	^{208}At	6.4± 1.8	-	-
^{123}Xe	11.9± 0.4	4.6± 0.4	6.2± 0.3	^{209}At	9.5± 0.2	-	-
^{124}Sb*	9.6± 0.3	1.90± 0.20	7.5± 0.3	^{210}At	6.0 ± 0.1	-	-
^{124}I	8.7± 0.1	2.3± 0.1	7.9± 0.2	^{211}Rn	5.0± 0.6	-	-

[a]The asterisk denotes a nuclide not used in computation of isobaric yields due to unknown yield of other members of isomeric pair.
[b]In mb.
[c]In mg/cm^2 Th.

W. F/B is a range-weighted measure of the fragment angular distributions, while $2W(F+B)$ is proportional to the fragment range (energy) [18].

Before proceeding to deduce other information from these data, we thought it might be useful to point out certain qualitative features of the primary data. In Fig. 2 we show a comparison of the values of the common "independent yield" nuclides seen in this work for the three projectile energies and the interaction of 3 GeV ^{12}C with ^{238}U [19]. (The ratios of the reaction cross sections [20] at the three argon energies is 0.92/1/0.97.) Since the "independent yield" nuclides sample a variety of reaction mechanisms and collision impact parameters, the data suggest no large changes occurring in reaction mechanism(s) between each pair of projectile energies but with some small changes in going from 44 to 95 MeV/nucleon. The similarity in reaction cross sections and expected linear momentum transfer (assuming a maximum linear

TABLE III. Nuclide yields and recoil properties for the interaction of 95 MeV/nucleon ^{36}Ar with ^{232}Th.

Nucleus[a]	Cross section[b]	F/B	$2W(F+B)$[c]	Nuclide	Cross section[b]	F/B	$2W(F+B)$[c]
^{24}Na	27.3± 0.5	31.5± 1.8	38.1± 0.9	^{121}Te^{m}	5.7± 0.8	3.2± 0.1	7.7± 0.1
^{28}Mg	8.6± 0.7	24.4± 2.4	33.0± 1.1	^{121}I	10.8± 0.3	7.8± 0.7	7.3± 0.3
^{38}S	1.4± 0.1	-	-	^{122}Sb	8.5± 0.1	1.9± 0.2	7.1± 0.3
^{42}K	8.5± 0.4	-	-	^{123}Te^{m*}	6.0± 0.1	2.4± 0.2	7.7± 0.4
^{44}Sc	0.8± 0.1	-	-	^{123}Xe	10.1± 0.3	6.2± 0.8	6.2± 0.3
^{44}Sc^{m}	3.1± 0.1	-	-	^{124}Sb	7.9± 0.6	1.82± 0.07	8.0± 0.1
^{46}Sc	10.0± 0.1	10.8± 0.2	16.9± 0.2	^{124}I	6.6± 0.2	2.9± 0.4	7.5± 0.5
^{47}Ca	2.1± 0.1	7.7± 0.8	15.5± 0.4	^{125}Xe	10.5± 0.3	-	-
^{47}Sc	10.3± 1.0	-	-	^{126}Sb*	4.5± 0.1	1.63± 0.05	8.2± 0.1
^{48}Sc	5.1± 0.2	6.3± 0.7	14.2± 0.9	^{126}I	6.1± 0.5	2.6± 0.3	7.7± 0.5
^{48}V	2.3± 0.1	11.5± 0.5	15.2± 0.2	^{126}Ba	6.3± 0.5	-	-
^{51}Cr	8.2± 0.2	7.0± 0.4	13.6± 0.4	^{127}Sb	6.0± 0.1	1.37± 0.11	7.6± 0.3
^{56}Mn	6.9± 0.4	5.4± 1.0	12.3± 0.8	^{127}Xe	15.4± 0.5	4.8± 0.7	0.53± 0.02
^{56}Co	0.5± 0.1	2.7± 0.3	18.3± 1.0	^{127}Cs	13.4± 0.3	5.2± 0.6	6.1± 0.3
^{58}Co	6.3± 0.1	7.3± 0.2	12.2± 0.2	^{128}Ba	7.1± 0.6	-	-
^{59}Fe	7.5± 0.1	4.0± 0.2	11.7± 0.2	^{129}Sb	2.3± 0.4	-	-
^{69}Zn^{m*}	5.0± 0.2	2.28± 0.19	12.2± 0.6	^{129}Cs	22.7± 2.1	-	-
^{71}Zn^{m*}	2.1± 0.1	2.12± 0.29	12.2± 0.8	^{130}I*	4.3± 0.1	1.40± 0.05	7.8± 0.4
^{71}As	3.1± 0.2	2.1± 0.3	12.4± 0.8	^{131}I	10.4± 0.1	1.49± 0.02	8.2± 0.1
^{74}As	10.0± 0.1	3.3± 0.1	10.0± 0.1	^{131}Ba	11.9± 1.1	6.9± 0.2	6.6± 0.1
^{75}Se	9.5± 0.5	4.5± 0.1	9.0± 0.1	^{132}Te	4.5± 0.5	1.62± 0.07	8.3± 0.2
^{75}Br	1.3± 0.1	-	-	^{132}I*	2.6± 0.8	1.24± 0.20	7.2± 0.6
^{76}As	16.9± 0.7	3.1± 0.3	9.8± 0.6	^{132}Cs	6.9± 0.1	2.16± 0.17	6.6± 0.3
^{77}Br	9.4± 0.6	-	-	^{132}La	8.6± 0.9	-	-
^{78}As	8.7± 0.4	2.10± 0.14	13.1± 0.4	^{132}Ce	7.6± 0.1	15.7± 3.6	6.4± 0.3
^{83}Rb	18.3± 0.4	3.6± 0.1	8.5± 0.1	^{133}I	8.0± 0.3	1.54± 0.14	9.7± 0.5
^{83}Sr	4.8± 0.6	-	-	^{135}I	6.5± 0.6	1.85± 0.27	8.9± 0.7
^{84}Rb	14.4± 0.2	2.7± 0.1	9.3± 0.1	^{135}Xe	7.3± 0.1	1.49± 0.19	7.4± 0.5
^{85}Sr*	20.3± 0.7	3.4± 0.3	9.9± 0.5	^{135}Ce	15.2± 2.9	4.2± 0.4	7.5± 0.4
^{86}Rb	20.8± 0.3	2.6± 0.1	7.8± 0.2	^{136}Cs*	3.3± 0.1	1.57± 0.05	7.5± 0.1
^{86}Y	8.1± 0.1	3.8± 0.4	7.9± 0.4	^{139}Ba	10.3± 0.4	1.54± 0.18	7.8± 0.5
^{87}Y	17.7± 0.1	3.9± 0.1	8.2± 0.1	^{139}Ce	12.8± 0.1	7.4± 0.1	5.7± 0.1
^{87}Y^{m}	15.9± 0.3	3.7± 0.3	8.2± 0.4	^{140}Ba	8.3 ± 0.2	1.49± 0.03	7.4± 0.1
^{87}Kr	12.2± 0.4	1.77± 0.20	6.9± 0.4	^{141}Ce	11.8 ± 0.1	1.60± 0.04	6.3± 0.1
^{88}Kr	11.0± 1.7	-	-	^{142}La	6.6± 0.3	1.97± 0.21	10.6± 0.6
^{88}Y	10.1± 0.9	3.1± 0.5	9.1± 0.8	^{143}Ce	7.2± 0.6	-	-
^{88}Zr	12.2± 0.2	5.0± 0.2	7.4± 0.2	^{145}Eu	6.3± 0.6	-	-
^{89}Zr	14.0± 0.3	4.2± 0.2	8.2± 0.2	^{146}Gd	8.2± 0.1	16.7± 1.7	4.7± 0.1
^{90}Y^{m*}	11.1± 1.4	2.26± 0.12	10.3± 0.4	^{147}Eu	8.0± 0.9	-	-
^{90}Nb	7.4± 0.1	5.8± 0.6	8.3± 0.3	^{147}Gd	12.1± 1.5	3.4± 0.5	5.3± 0.4
^{91}Sr	23.1± 1.4	1.53± 0.08	12.3± 0.3	^{148}Eu	1.7 ± 0.1	-	-
^{92}Sr	17.1± 0.2	1.41± 0.05	10.7± 0.2	^{149}Gd	10.3± 0.1	-	-
^{92}Y	20.4± 1.4	-	-	^{151}Tb	9.4± 1.1	-	-
^{92}Nb^{m*}	1.2± 0.1	3.3± 0.3	9.8± 0.5	^{152}Tb	8.9± 0.5	-	-
^{93}Y	36.9± 2.1	-	-	^{152}Dy	3.9± 0.6	-	-
^{93}Mo^{m*}	4.9± 0.1	4.3± 0.5	8.3± 0.4	^{153}Tb	6.6± 1.4	-	-
^{95}Zr	32.0± 1.1	1.48± 0.02	9.6± 0.1	^{155}Tb	11.0 ± 3.0	-	-
^{95}Nb^{m*}	19.9± 0.7	1.23± 0.11	10.2± 0.5	^{155} Dy	7.2± 0.4	-	-
^{95}Tc*	8.8± 0.3	5.0± 0.5	8.0± 0.5	^{157}Dy	9.7± 0.1	8.0± 0.7	6.0± 0.3
^{96}Nb	14.2± 0.7	2.18± 0.22	8.4±0.5	^{158}Er	6.8± 0.4	-	-
^{96}Tc*	7.60±0.11	4.4± 0.2	7.6± 0.1	^{160}Er	9.7± 0.4	-	-
^{97}Zr	21.3± 0.3	1.41± 0.20	11.3± 0.9	^{167}Tm	8.5 ± 0.1	-	-
^{97}Nb*	11.7± 1.7	1.67± 0.22	10.2± 0.7	^{169}Yb	8.2±1.0	19.2±1.8	4.1±0.1
^{97}Ru	6.1± 0.1	4.5± 0.6	9.4± 0.7	^{169}Lu	8.4± 0.6	-	-
^{99}Mo	37.3± 0.1	1.68± 0.02	10.0± 0.1	^{170}Hf	6.1 ± 0.5	-	-
^{99}Rh^{m*}	3.7± 0.1	5.1± 0.9	10.0± 0.7	^{171}Lu	8.3± 0.1	-	-
^{100}Rh	7.9± 1.1	6.7± 1.0	6.4± 0.5	^{171}Hf	10.0± 0.4	-	-
^{101}Rh^{m*}	10.0± 0.2	4.8± 0.2	8.0± 0.2	^{173}Hf	10.6± 3.2	-	-
^{103}Ru	50.9± 0.6	1.73± 0.04	9.4± 0.1	^{175}Hf	9.9 ± 0.6	-	-
^{105}Ru	36.3± 0.4	1.58± 0.09	10.3± 0.3	^{177}W	3.8 ± 0.1	-	-

TABLE III. (*Continued*).

Nucleus[a]	Cross section[b]	F/B	$2W(F+B)$[c]	Nuclide	Cross section[b]	F/B	$2W(F+B)$[c]
^{105}Rh*	52.4± 3.7	1.85± 0.28	8.8± 0.7	^{181}Re	9.2± 0.4	-	-
^{106}Rh^{m*}	10.9± 0.6	2.05± 0.28	9.2± 0.7	^{182} Os	5.0± 1.0	-	-
^{106}Ag^{m*}	6.5± 0.3	4.1± 0.2	7.6± 0.2	^{183}Re	5.4± 0.2	-	-
^{109}In	10.1± 0.8	-	-	^{184}Ir	5.3± 1.0	-	-
^{110}Ag^{m*}	9.7± 0.6	2.5± 0.1	9.2± 0.2	^{185}Os	6.7± 0.2	-	-
^{111}In	12.5± 0.1	5.3± 0.3	8.0± 0.3	^{186}Pt	3.2± 0.1	-	-
^{115}Cd*	20.5± 0.2	1.64± 0.16	9.1± 0.4	^{188}Pt	4.6± 0.3	-	-
^{116}Te	5.4± 0.8	-	-	^{192}Hg	4.2± 0.2	-	-
^{117}Cd	5.1± 1.5	-	-	^{199}Pb	5.2± 0.3	-	-
^{117}Cd^{m}	14.8± 3.0	1.63± 0.09	9.6± 0.3	^{200}Tl	3.6± 0.4	-	-
^{117}Te	8.8± 0.4	-	-	^{200}Pb	4.2± 0.1	-	-
^{118}Sb^{m*}	6.2± 0.4	3.2± 0.2	7.5± 0.3	^{201}Pb	3.9± 0.2	-	-
^{119}Te	7.0± 0.2	6.2± 1.2	7.2± 0.4	^{202}Tl	4.0± 0.1	-	-
^{119}Te^{m}	5.4± 0.1	4.8± 0.6	6.7± 0.3	^{202}Bi	4.1± 0.6	-	-
^{120}Sb*	6.3± 0.1	2.4± 0.1	8.0± 0.1	^{203}Pb	4.9± 0.2	-	-
^{121}Te	10.4± 0.1	5.8± 0.3	5.9± 0.1				

[a]The asterisk denotes a nuclide not used in computation of isobaric yields due to unknown yield of other members of isomeric pair.
[b]In mb.
[c]In mg/cm^2 Th.

momentum transfer [21,22] of 180 MeV/c per projectile nucleon) between the three argon energies would lead one to expect that there would be no large changes in reaction mechanism with increasing projectile energy in this energy range.

Examination of the data in Fig. 2(c) shows the larger linear momentum (and energy) transfer in the argon-induced reaction (compared to the carbon-induced reaction) produces lower Z nuclei (after preequilibrium emission) that fission and produces more intermediate mass fragments.

To more fully utilize the cross-section data shown in Tables I, II, and III we have deduced mass-yield (isobaric yield) distributions from the measured formation cross sections. The method employed in this estimation procedure has been discussed previously [23].

The measured nuclidic formation cross sections were placed in 14 groups according to mass number. These cross sections were corrected for precursor beta or alpha decay, where necessary, by assuming that the independent yield cross sections for a given species, $\sigma(Z,A)$, can be expressed as a function of the isobaric yield $\sigma(A)$ as

$$\sigma(Z,A) = 0.5\sigma(A)[\mathrm{erf}(u) - \mathrm{erf}(w)], \quad (1)$$

where

$$u = (Z - Z_{mp} + 0.5)/C_z(A)\sqrt{2} \quad (2)$$

and

$$w = (Z - Z_{mp} - 0.5)/C_z(A)\sqrt{2}. \quad (3)$$

Here $C_z(A)$ is the Gaussian width parameter for mass number A, erf(x) is the error function of x, and $Z_{mp}(A)$ is the most probable atomic number for that A. Using this assumption and the further assumption that $\sigma(A)$ varies slowly and smoothly as a function of A [allowing data from adjacent isobars to be combined in determining $Z_{mp}(A)$ and $C_z(A)$] , one can use the laws of radioactive decay to iteratively correct the measured cumulative formation cross sections for precursor decay.

Within each group, the data were fitted by a Gaussian-shaped independent yield distribution. (Only nuclides with well-characterized beta- or alpha-decay precursors and well-understood members of an isomeric pair were included in the analysis.) The nuclide groupings along with the centers and widths of the Gaussian distributions are given in Tables IV, V, and VI. The independent yield distributions deduced from the measured formation cross sections are shown in Figs. 3, 4, and 5. The deduced values of Z_{mp}/A are uncertain to 0.005 unit while those of C_z are typically uncertain to 0.1 Z unit.

The centers and widths of the Gaussian distributions are (within the uncertainties) similar at the three projectile energies. As has been observed in the fragmentation of ^{238}U by intermediate energy and relativistic heavy ions [19] and protons [24,25], many Gaussian distributions are double-humped with a neutron-rich and neutron-deficient component. For example, the observed distributions in this work are in qualitative agreement with the observed Cs isotopic distribution [26] from the reaction of 77 MeV/nucleon ^{12}C with ^{238}U. It has been shown previously [25,27] that two separate reaction mechanisms, a deep spallation process, and low energy binary fission, contribute to the production of the n-deficient and n-rich components of these charge distributions. The widths of the charge distributions above mass number 190 are not well defined by the data. We have chosen to simply use the charge distribution widths that characterized the lower mass regions for this region. [Use of a broader

charge distribution (σ = 1.0 instead of σ =0.6) would increase the yields of the nuclei with $A > 190$ by a factor of 10–25 % which is within the estimated uncertainty (see below) of 30% in the integrated yields.]

The isobaric yield distributions obtained from integrating the independent yield distributions for each individual A value are shown in Fig. 6. The distributions are dominated by a broad central bump (thought to be due, in part, to fission) with lesser yields of the intermediate mass fragments ($A < 60$) and the heavy residues ($A > 150$). Integration of these distributions gives cross sections of 2010, 1470, and 1280 mb for IMFs ($A = 24 - 60$), 3600, 2700, and 2340 mb for fission ($A = 60 - 150$, multiplicity 2) and 790, 790, and 710 mb for heavy residues ($A = 150 - 211$) for the 44 MeV/nucleon, 77 MeV/nucleon, and 95 MeV/nucleon reactions, respectively. The sums of these cross sections, 6400, 4960, and 4330 mb are greater than the reaction cross sections [20], 5020, 5480, and 5330 mb for the 44

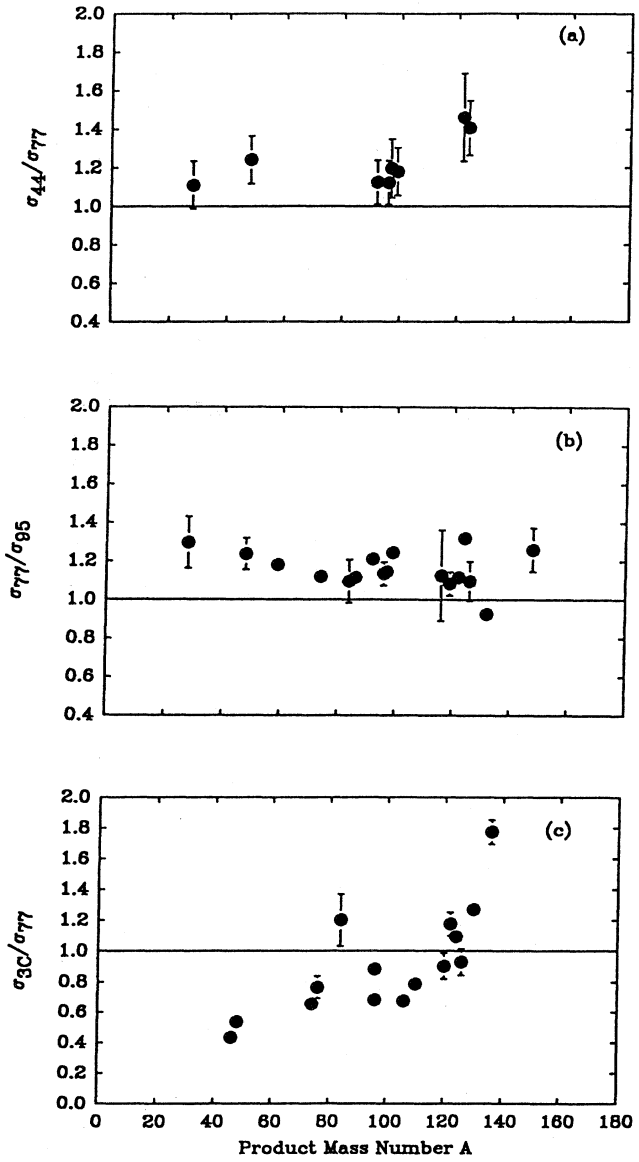

FIG. 2. Plot of the ratios of the "independent yield" nuclidic production cross sections for the interaction of (a) 44 and 77 MeV/nucleon Ar with ^{232}Th; (b) 77 and 95 MeV/nucleon Ar with ^{232}Th; (c) 3 GeV ^{12}C with ^{238}U and 3.1 GeV ^{40}Ar with ^{232}Th.

TABLE IV. Charge dispersion parameters for the reaction of 44 MeV/nucleon ^{40}Ar with ^{232}Th. The last two columns give the relative heights of the two components in the case of double Gaussian charge distributions and whether they represent neutron-rich or neutron-deficient distributions.

Mass number range	σ_A	a	b	Relative height	Neutron excess
24–38	0.6	1.310	0.427		
42–56	0.6	1.240	0.427		
71–79	0.6	2.380	0.400	1.000	Rich
71–79	0.6	1.460	0.427	1.000	Deficient
83–92	0.8	3.740	0.383	1.000	Rich
83–92	0.6	2.050	0.421	0.489	Deficient
93–105	1.0	4.280	0.377	1.000	Rich
93–105	1.0	3.255	0.408	0.429	Deficient
111–121	1.0	4.450	0.373	1.000	Rich
111–121	1.0	4.320	0.399	0.714	Deficient
122–129	1.0	5.040	0.368	0.800	Rich
122–129	1.0	5.280	0.392	1.000	Deficient
131–140	1.0	5.720	0.361	1.000	Rich
131–140	1.0	7.120	0.381	0.963	Deficient
142–149	0.6	6.160	0.356	0.786	Rich
142–149	0.6	7.630	0.379	1.000	Deficient
151–161	0.6	9.860	0.364		
165–177	0.6	11.800	0.350		
181–192	0.6	15.200	0.334		
199–205	0.6	18.560	0.316		

TABLE V. Charge dispersion parameters for the reaction of 77 MeV/nucleon ^{40}Ar with ^{232}Th.

Mass number range	σ_A	a	b	Relative height	Neutron excess
24–38	0.6	1.310	0.427		
42–59	0.6	1.240	0.427		
71–78	0.6	2.220	0.400	1.000	Rich
71–78	0.6	1.460	0.427	0.923	Deficient
83–92	1.0	3.600	0.382	1.000	Rich
83–92	0.6	2.050	0.421	0.555	Deficient
93–105	1.0	4.280	0.377	1.000	Rich
93–105	1.0	3.255	0.408	0.378	Deficient
109–121	1.0	4.450	0.373	1.000	Rich
109–121	1.0	3.920	0.403	0.690	Deficient
122–129	1.0	5.600	0.367	1.000	Rich
122–129	1.0	5.280	0.392	1.00	Deficient
131–140	1.2	5.720	0.361	1.000	Rich
131–140	1.0	7.120	0.381	1.000	Deficient
141–149	1.0	6.720	0.356	1.000	Rich
141–149	0.6	8.480	0.377	0.933	Deficient
151–160	0.6	9.860	0.364		
167–177	0.6	11.800	0.350		
181–192	0.6	15.120	0.334		
199–205	0.6	18.560	0.316		

TABLE VI. Charge dispersion parameters for the reaction of 95 MeV/nucleon ^{36}Ar with ^{232}Th.

Mass number range	σ_A	a	b	Relative height	Neutron excess
24–38	0.6	1.310	0.427		
42–59	0.6	1.240	0.427		
71–78	0.6	2.220	0.400	1.000	Rich
71–78	0.6	1.620	0.427	0.733	Deficient
83–92	1.0	3.600	0.382	1.000	Rich
83–92	0.6	2.050	0.421	0.648	Deficient
93–105	1.0	4.180	0.377	1.000	Rich
93–105	1.0	3.255	0.408	0.378	Deficient
109–121	1.0	4.450	0.373	1.000	Rich
109–121	1.0	3.920	0.403	0.800	Deficient
122–129	1.0	5.600	0.367	1.000	Rich
122–129	1.0	5.280	0.392	0.933	Deficient
131–140	1.2	5.720	0.361	1.000	Rich
131–140	1.0	7.120	0.381	0.963	Deficient
141–149	1.0	6.720	0.356	0.786	Rich
141–149	0.6	8.480	0.377	1.000	Deficient
151–160	0.6	9.860	0.364		
167–177	0.6	11.620	0.350		
181–192	0.6	15.200	0.334		
199–205	0.6	18.400	0.316		

MeV/nucleon, 77 MeV/nucleon, and 95 MeV/nucleon reactions, respectively. Since our integration of the mass yields should be a lower limit on the reaction cross section because we neglect fragments with $A < 24$, we assume that some IMFs have heavy residue partners. This would lead to a double counting in our simplistic accounting. Nonetheless, the heavy residue events certainly have multiplicity of unity, and there are associated cross sections of 790, 790, and 710 mb for the three projectile energies. These measured heavy residue cross sections exceed those observed by Pollacco *et al.* [12] for the same reaction (250 and 230 mb for the 44 and 77 MeV/nucleon reactions), presumably due to the high thresholds for residue detection in their experiment. (The total uncertainty in these integrated cross sections is about 30% [23].)

These heavy residue formation cross sections are quite surprisingly large, given the fissionable nature of the target nucleus and any composite nuclei formed in the reaction. The heavy residue formation cross sections in this work, representing $\sim$ 15% of the total reaction cross section, are similar to those observed for the reaction [19] of 3.0 GeV ^{12}C with ^{238}U (where the heavy residue cross sections were $\sim$ 16% of the total reaction cross section). This is yet another example of the total kinetic energy scaling of reaction product yields [29]. Two seemingly contradictory statements can be made about the magnitude of the heavy residue cross sections compared with those expected for fusion and fusionlike events. The values of the heavy residue cross sections exceed any projected complete fusion cross section calculated using the proximity potential [28] by an order of magnitude, but they are of similar magnitude (770 mb vs 760 mb) as the cross section associated with the fusionlike events in the folding angle distribution in the reaction of 31 MeV/nucleon ^{40}Ar+^{232}Th [2]. Of course, the terms "complete fusion" and "fusionlike" refer to very different components of the reaction cross section in systems where the maximum linear momentum transfer is 48% of

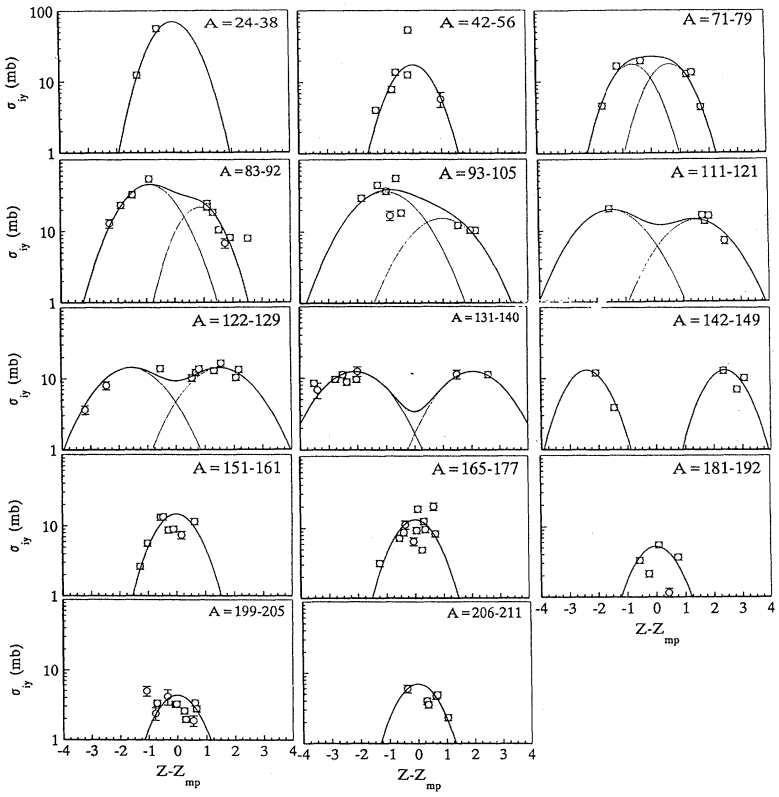

FIG. 3. The fragment independent yield distributions from the interaction of 44 MeV/nucleon ^{40}Ar with ^{232}Th. The plotted points are the independent yield cross sections calculated from the data while the solid lines are the Gaussian charge dispersions used in the calculation.

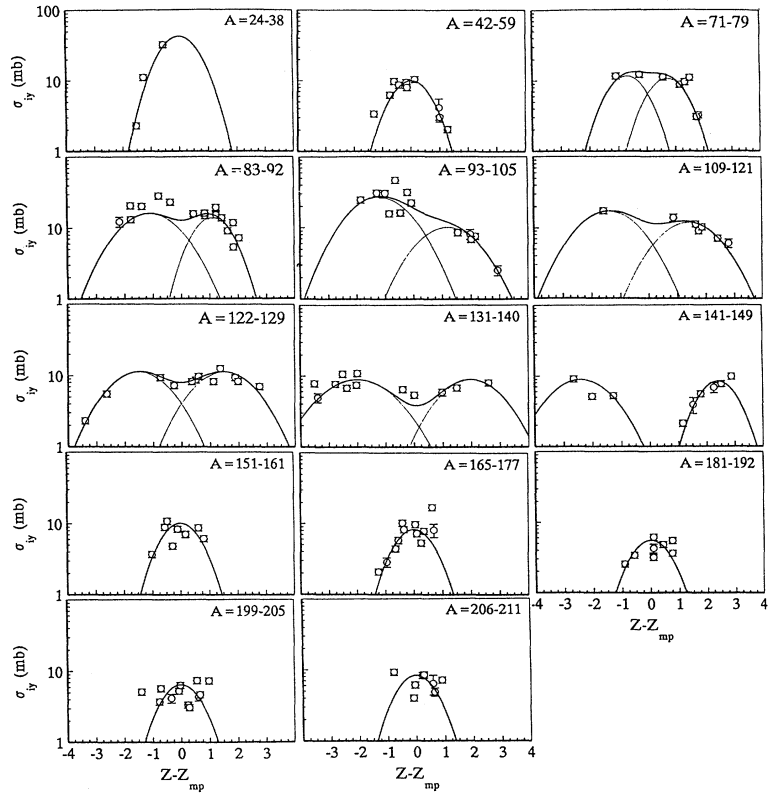

FIG. 4. Same as Fig. 3 except system is 77 MeV/nucleon $^{40}Ar+^{232}Th$.

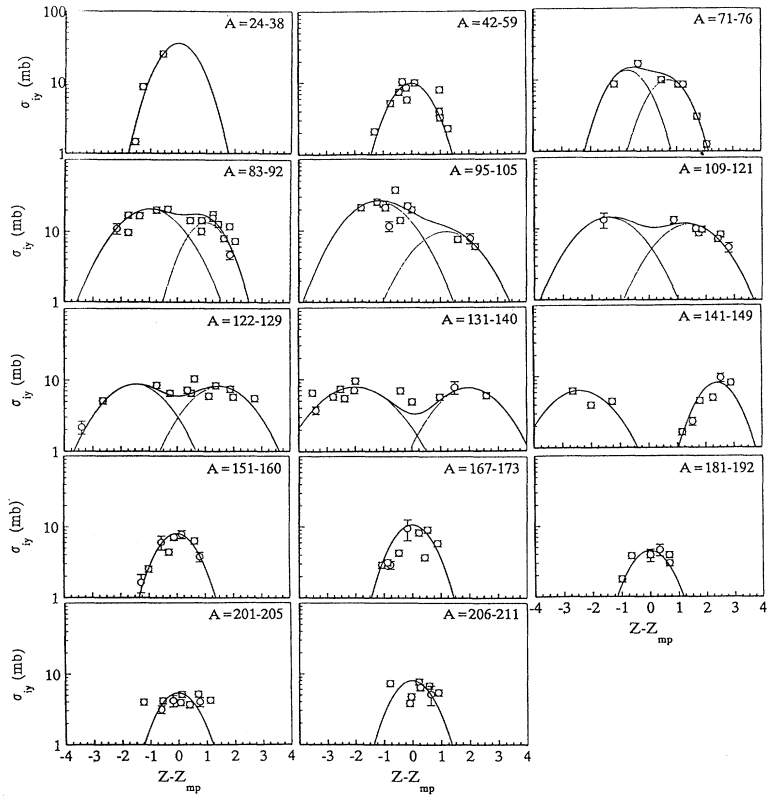

FIG. 5. Same as Fig. 3 except system is 95 MeV/nucleon $^{36}Ar+^{232}Th$.

full momentum transfer [21,22].

However, we can better define our observations by noting that, besides the cross sections for various processes, we also have information about the recoil properties of the reaction products. To interpret these measured recoil properties in physically meaningful quantities, we have used mostly the integral catcher analysis method of Tobin and Karol [30]. In this analysis, we assume the final velocity of each fragment in the laboratory system can be written as $V_{\rm lab} = V + v$ where the velocity v is the velocity kick given to the fragment during the primary stage of the reaction and V is an average isotropic recoil velocity due to either sequential particle emission or fission. Since it is further assumed that $v = v_{\|}$, the average projection of the initial fragment velocity distribution on the beam axis, then V also includes an isotropic component of the velocity distribution in the initial stage of the reaction. (The case where there is a transverse velocity kick given in the initial stage of the reaction, is not considered, although values of $v_{\perp} = 0.25 v_{\|}$ have been shown [30] not to affect the analysis. Furthermore, Crespo, Alexander, and Hyde [31] have shown that due to canceling errors, the value of $v_{\|}$ is practically independent of $v_{\perp}/V$.) As opposed to a conventional analysis of recoil data, the Tobin-Karol method imposed no constraints on target thickness and corrected certain limitations and deficiencies in the conventional analysis.

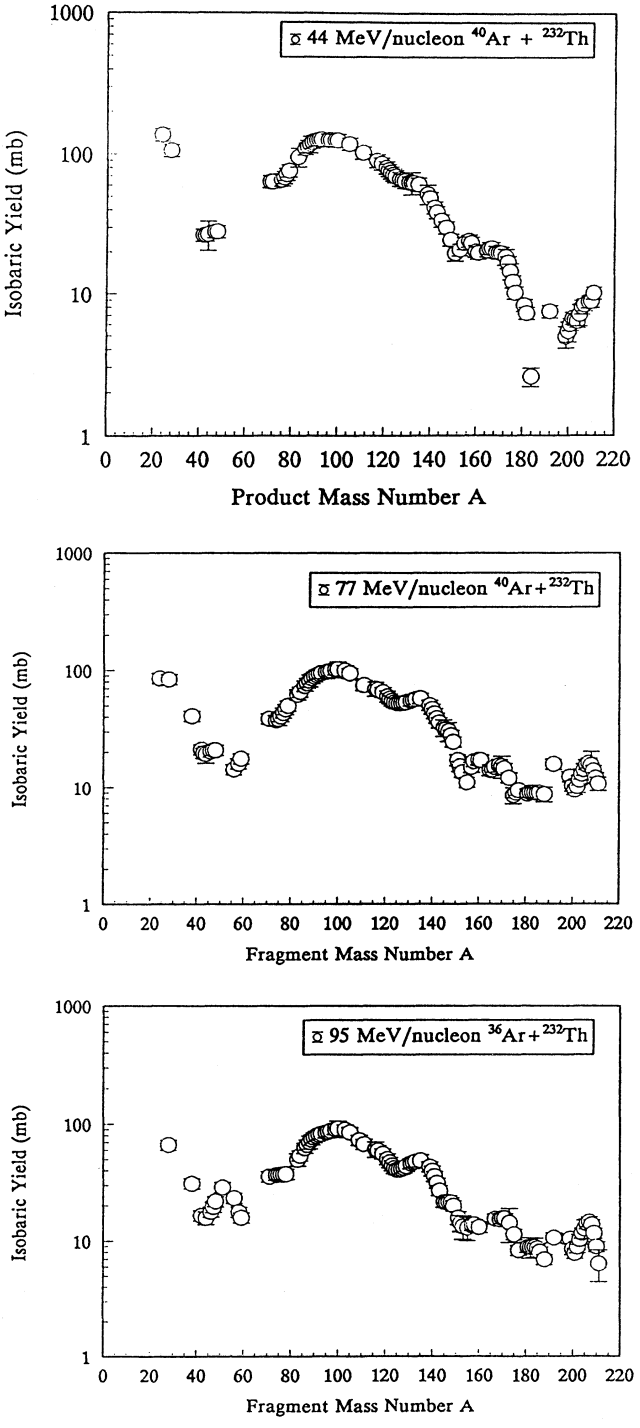

FIG. 6. Fragment isobaric yield distributions for the interaction of 44 and 77 MeV/nucleon ^{40}Ar and 95 MeV/nucleon ^{36}Ar with ^{232}Th.

To get similar information about the heaviest reaction products is not possible from the Tobin-Karol method because of the large values of F/B for these products and the difficulties in measuring this quantity. However, it has been shown [32], for intermediate energy heavy ion reactions, that the forward range, FW, can be used to calculate values of the quantity $v_{\|}$. This was done for the products with $A \geq 150$, where the average lower limit on F/B was 75, in the two higher energy bombardments. No such information could be derived at 44 MeV/nucleon because of the use of a thinner target.

The results of the recoil analysis, for each nuclide whose recoil properties were observed, are shown in Fig. 7. The values for the fractional linear momentum transfer were calculated from the values of $v_{\|}/v_{CN}$ using the massive transfer assumption. The mean FLMT values for the fission region ($A = 60 - 150$) were 0.10, 0.086, and 0.086 for the three projectile energies while the mean FLMT values for the residue region ($A > 150$) were 0.14, 0.12, and 0.13, respectively, for the 44, 77, and 95 MeV/nucleon experiments. The mean FLMT values for fission fragments agree generally with the most probable fractional linear momentum transfer of 0.07 measured for the 44 MeV/nucleon ^{40}Ar+^{232}Th reaction [1] using the folding angle technique. The values of the FLMT for the fission fragments and heavy residues are considerably lower than those values expected from the systematics of fusionlike collisions (0.63, 0.48, 0.43) and those expected from a simple Boltzmann master equation preequilibrium model [33] calculation (0.51, 0.28, 0.22) for the 44, 77, and 95 MeV/nucleon reactions. This seems to clearly show that most of these fragments do not originate in fusionlike collisions. One recognizes that this finding does not contradict observations [10–12] of highly excited evaporation residues but points out that these highly excited residues are atypical. Larger momentum transfers are observed for events leading to multifragmentation ($A < 60$) events at the two higher energies, suggesting these events correspond to fusionlike collisions. The very large momentum transfers associated with the

formation of Na and Mg fragments may have to be viewed with caution since such events could be degraded projectilelike fragments.

The values of V, the velocity kick imparted to the products of the primary projectile-target interaction by fission or particle evaporation, are compared to what one expects for the fission of a thoriumlike nucleus in Fig. 8 for the 77 MeV/nucleon data. (Similar data exist for the other energies.) The observed values of V for the $A = 60 - 150$ nuclei are about 70% of those expected from binary fission. Even the fragments resulting from the most peripheral collisions ($N/Z = 1.4 - 1.5$, see below) do not have V values typical of the binary fission of a Th-like nucleus. One could speculate that what appears to be a normal fissionlike bump in the fragment mass distributions (Fig. 5) corresponds to a system whose scission configuration is elongated by 30% relative to a normal scission configuration or is a combination of reaction mechanisms, such as spallation and fission [27].

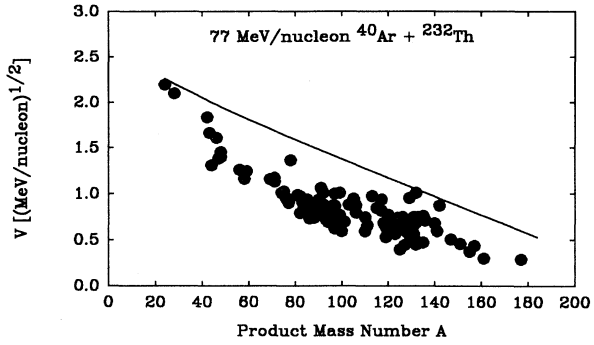

FIG. 8. The velocity V in the frame of the struck nucleus of the fragments form the interaction of 77 MeV/nucleon ^{40}Ar with ^{232}Th. The line represents the calculated fragment velocities assuming they resulted from the fission of ^{232}Th.

In each section of Fig. 7 there is a large spread in values for a given value of the fragment mass number A, particularly for fission fragments. Some of this spread is due to the changes in recoil properties with fragment N/Z (Fig. 9). The more n-deficient fission fragments (for a given A) result from higher momentum transfer events. For the heavy residues, the dependence is less pronounced but still significant.

IV. DISCUSSION

Success in describing intermediate energy nuclear collisions has been achieved by models based upon a transport equation, the Boltzmann-Uehling-Uhlenbeck (BUU)

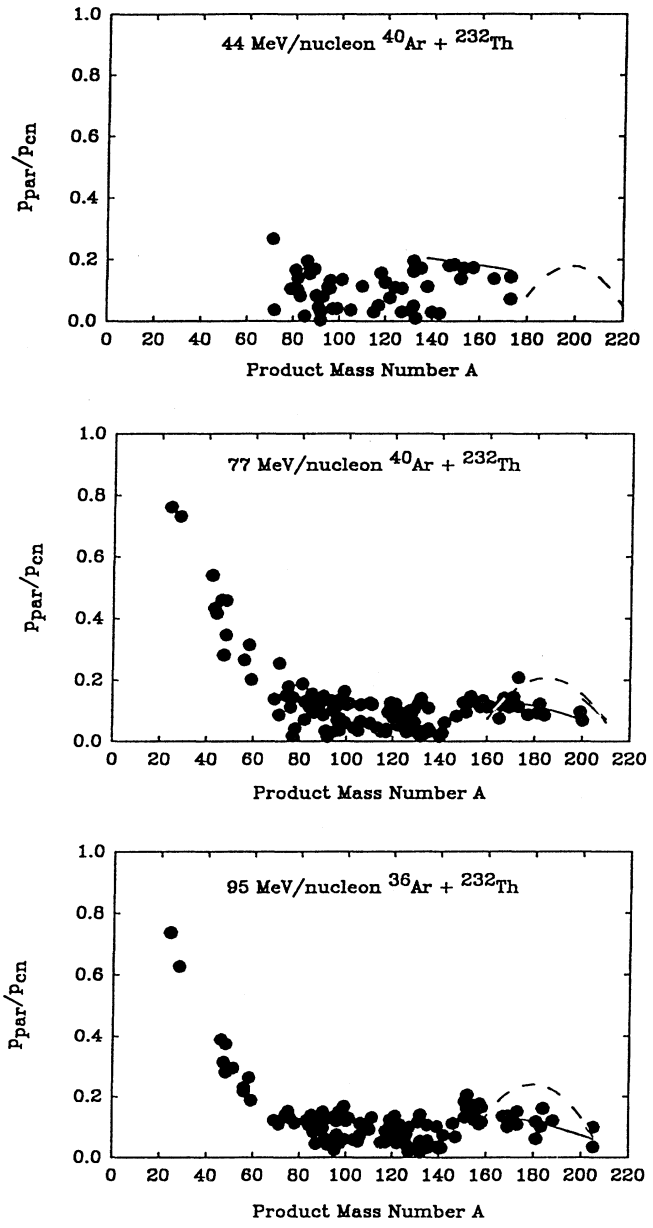

FIG. 7. Longitudinal fragment momenta for the reactions studied in this work. The plotted points are the experimental data, the solid and dashed lines are the prediction of the BUU and INC models, respectively.

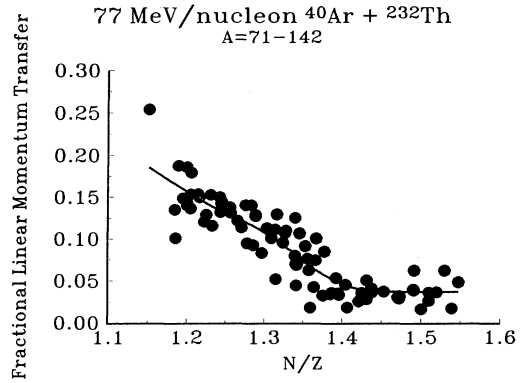

FIG. 9. The N/Z dependence of the fragment longitudinal momenta for fragments with 71 ¡ A ¡ 142 from the interaction of 77 MeV/nucleon ^{40}Ar + ^{232}Th. The solid line is a loess fit to the data.

equation. In this equation, the phase space distribution function $f(r, p, t)$ of the reacting system is assumed to change only due to collisions, with the forces involved being derived from a nuclear potential, U, i.e.,

$$\frac{\partial f}{\partial t} + v \cdot \nabla_r f - \nabla_r U \cdot \nabla_p f = \int \frac{d^3p_2 d^3p_1' d^3p_2' \sigma v_{12}}{(2\pi)^6} [f f_2 (1 - f_1')(1 - f_2') - f_1' f_2' (1 - f)(1 - f_2)] \delta^3(p + p_2 - p_1' p_2'), \quad (4)$$

where ∇_r and ∇_p are the gradients with respect to r and p, σ is the free nucleon-nucleon scattering cross section, and v_{12} is the relative velocity of the colliding nucleons.

The density dependent nuclear potential U is frequently taken to be of the Skyrme form

$$U = -356 \text{ MeV} \left(\frac{\rho}{\rho_0}\right) + 303 \text{ MeV} \left(\frac{\rho}{\rho_0}\right)^{\frac{7}{6}} \quad (5)$$

which corresponds to a "soft" equation of state ($K = 200$ MeV). Neglect of the potential terms in the equation corresponds to the intranuclear cascade (INC) model. The BUU equation thus includes both the mean-field and nucleon-nucleon collision terms appropriate for the transitional intermediate energy regime while the INC model includes only the effects of nucleon-nucleon scattering known to be important at higher energies. In an attempt to understand the data described in Sec. III we have used both the BUU model and the INC model to simulate the collisions of 44, 77, and 95 MeV/nucleon Ar with ^{232}Th. We have used the numerical implementation of the BUU model developed by Bauer [34] for the BUU model calculations. We have assumed a soft equation of state ($K = 200$) and followed the evolution of the collisions for $b = 0...14$ fm in 0.5 fm steps for times of 0 to 200 fm/c in steps of 5 fm/c, using 75 test particles per nucleon. At a time of 120 fm/c we stopped the BUU calculation and calculated the values of Z, A, J, E^*, and p of the targetlike residue. The deexcitation of the residue by fission or particle emission was calculated using a modified version of the PACE code that has been described previously [35,36] (see below).

Following the lead of Blaich *et al.* [36] we also used the INC model to simulate the production of primary targetlike residues in these collisions. We did so to understand the effect of neglecting mean-field terms in the BUU equation for these reactions and because the INC model is a traditional model that has been widely applied to the study of higher energy nuclear collisions. We have used the INC model of Yariv and Fraenkel [37] to simulate the Ar-Th collisions for impact parameters of 0...14, fm in 0.5 fm steps using 1000 cascades for each impact parameter. This calculation resulted in an estimation of the Z, A, J, E^*, p of each primary targetlike residue and the distribution of these quantities.

As mentioned previously we used a modified version of PACE to calculate the deexcitation of the residues from these two model simulations. In doing so we have made all the assumptions outlined by Blaich *et al.* First, we have assumed all residues with $E^* > 1000$ MeV will undergo multifragmentation and we ignore these events (which constituted $< 5\%$ of the events). For residues with E^* between 300 and 1000 MeV, we assume a fast nucleon cascade deexcites the fragments. When the residue excitation energy is 300 MeV or lower (by the result of fast nucleon emission or due to an original excitation) the deexcitation process is then described by the standard PACE code [35]. The known retardation of fission relative to particle emission at higher excitation energies is simulated by not allowing fission to compete with particle emission as a deexcitation mode until the excitation energy is about 150 MeV. (This corresponds roughly to a temperature of the residue of about 2 MeV and is consistent with estimates of when the neutron emission and fission time scales become equivalent for heavy nuclei. This parameter was varied from 75 to 200 MeV in several calculations and did not affect the qualitative conclusions drawn from the analysis.) At excitation energies below 150 MeV, fission was allowed as a decay channel in the PACE calculations. Fissility dependent values of a_f/a_n [38,39] were used in the fission calculation.

In Fig. 10 we show the primary targetlike residue distributions predicted by the two collision models for the reaction of 77 MeV/nucleon ^{40}Ar with ^{232}Th. In a manner that is reminiscent of the situation in relativistic heavy ion reactions [40], one observes substantial differences in the prediction of the two models for the primary product distributions. The INC model predicts a narrow A range of the primary products with very high excitation energies, longitudinal momenta and spins while the BUU model predicts a larger A range of primary products with lower values of E^*, $p_\parallel$, and J, except for the peripheral collisions where the BUU model predicts comparable or higher values for the transferred quantities.

For the study of heavy residues formed in these collisions and their properties, it turns out that these differences in predicted properties in peripheral collisions are important. This can be shown in many ways. In Fig. 7 we show the predicted values of the residue longitudinal momenta as calculated in the two models. The values predicted by the BUU model are in good agreement with the data while the INC model predictions differ from the observations. One also sees the BUU simulation correctly reproduces the decreasing residue momenta with increasing projectile energy.

One can also calculate the yield of secondary fragments with product mass numbers $60 \leq A \leq 150$ ("fission") and those with $150 \leq A \leq 220$ ("residues"). These data are shown in Table VII along with the measured values of these quantities. Again, the INC model is found to do a poorer job of describing the data although neither model does very good job of predicting the relative fission and residue yields. It appears that for 40–100 MeV/nucleon Ar-Th collisions at large impact parameters, the neglect of the mean field in the INC calculation is inappropriate for describing these collisions. This was demonstrated in a simulation for the 77 MeV/nucleon reaction where the mean field was "turned off" in a BUU simulation

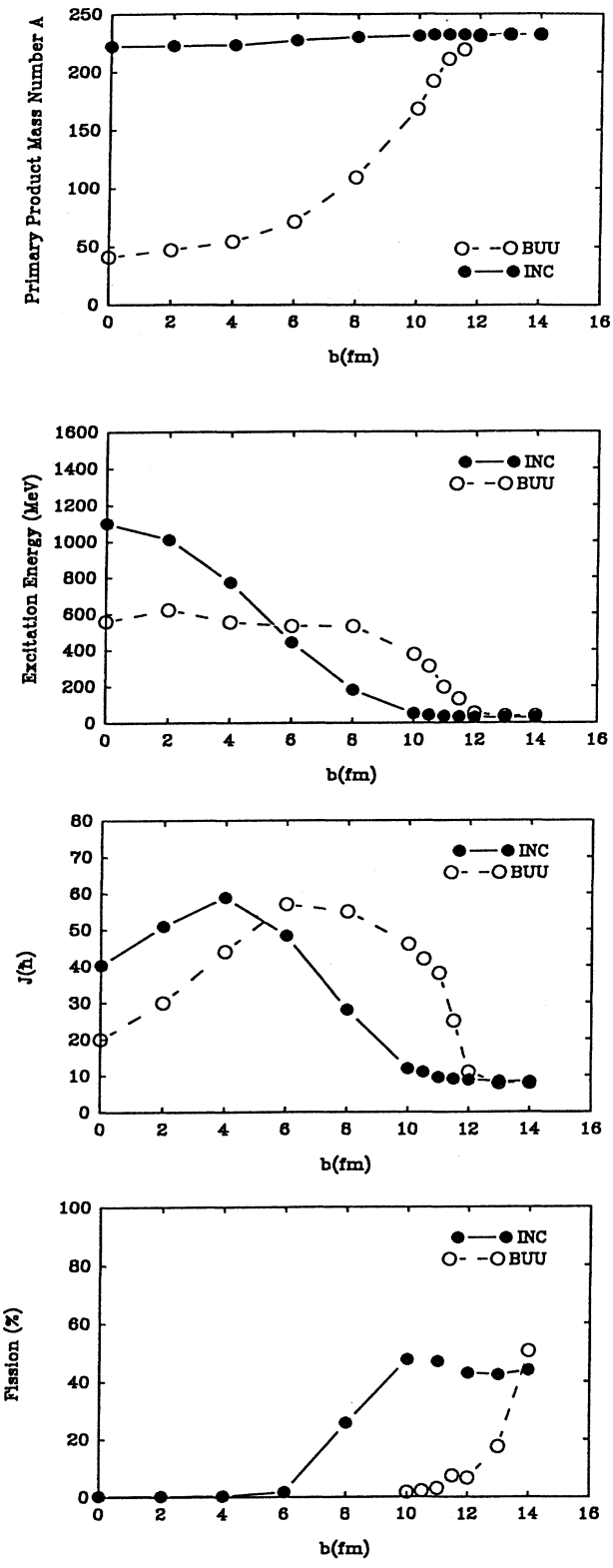

FIG. 10. The primary targetlike fragment properties as a function of impact parameter b for the 77 MeV/nucleon ^{40}Ar+^{232}Th reaction as calculated in the BUU and INC models.

TABLE VII. Comparison of BUU and INC predictions of the "fission/residue" ratio for Ar-Th collisions.

Beam energy (MeV/nucleon)	INC	BUU	Measured
44	1.0	2.4	4.6
77	0.7	2.0	3.4
95	0.7	1.4	3.3

giving an identical result as that obtained from the INC calculation.

Having shown the suitability of the BUU model for simulating the reactions studied in this work, we can use this model to help us understand how these low momenta residues are produced in copious yield in a reaction with a fissionable target, such as ^{232}Th. In Fig. 10 we show the percentage of nuclei that fission as a function of impact parameter. Remembering the increased weighting of large impact parameters in single particle inclusive measurements, we see that fission results primarily from the largest impact parameters (and correspondingly low momentum transfer). Qualitatively this is due to the retardation of fission at high excitation (smaller impact parameters) and the decreased fissility of the primary products resulting from smaller impact parameter collisions. In this context, it is difficult to understand the observation of Galin *et al.*, that the cross section for "fission following large momentum transfers" in the 44 MeV ^{40}Ar+^{232}Th reaction is 1.8 b [41] which, in turn, does not agree with the work of Conjeaud *et al.* [2]. The surviving residues arise, in the BUU simulations, from a limited range of impact parameters, b =9–11.5 fm. In a typical scenario about 10 neutrons are emitted along with about 5 α particles and a few protons to reach the A =160 (b =10.5 fm) to A = 210 (b =11.5 fm) residues. The p/α ratio in the production of an A = 180 residue is about 1/5. There are residues with $A \leq 150$, produced by multiple particle emission. Qualitatively, this is the origin of the N/Z dependence of the $(p_{\|}/p_{CN})$ ratio of the "fission products" shown in Fig. 9.

In Fig. 11 we show the density profiles of the colliding nuclei for the 77 MeV/nucleon ^{40}Ar+^{232}Th reaction as a function of impact parameter b and collision time t. The targetlike residues are formed in intermediate impact parameter collisions and peripheral collisions (whereupon they later fission). For central collisions (b = 0–3 fm) unusual odd-shaped extended composite nuclei are formed. Most likely these nuclei will break up into multiple fragments and are the primary result of fusionlike collisions (Fig. 7).

V. CONCLUSIONS

What have we learned from these measurements and the simulations? The conclusions of this paper are the following.

(a) Substantial yields of heavy residues ($\sim$ 0.8 b) are found in the interaction of 44–95 MeV/nucleon Ar with fissionable ^{232}Th. The use of radiochemical techniques

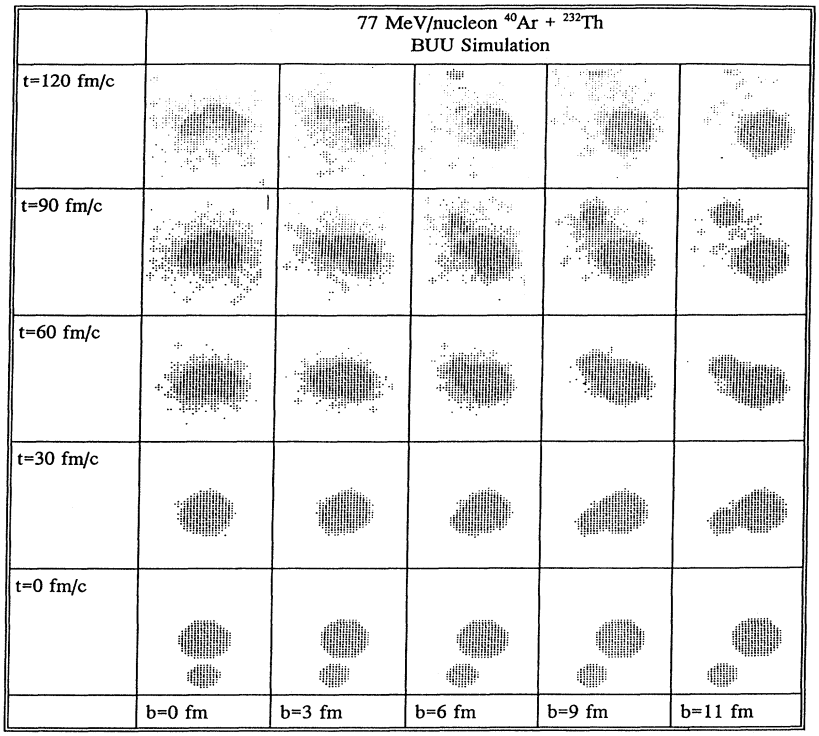

FIG. 11. Plots of the density distributions as a function of impact parameter b and time t as calculated in a BUU model simulation of the reaction of 77 MeV/nucleon ^{40}Ar with ^{232}Th.

has allowed one to detect residues that were missed in other measurements.

(b) The average momenta of these residues are low indicating they are not "where all the fusionlike events have gone" in the Ar-Th system. The "missing" fusionlike events have primarily gone into multifragmentation.

(c) The neglect of mean-field effects in the INC model makes it inappropriate for simulating intermediate energy (40–100 MeV/nucleon) collisions involving fissionable targets.

(d) The BUU model appears to do a good job of predicting the observed residue properties although further refinements are needed to give predictions that agree exactly with the data.

(e) The surviving residues are the result of retardation of fission coupled with charged particle emission.

ACKNOWLEDGMENTS

We wish to thank W. Bauer and M. Fauerbach for providing us with the BUU, and INC/PACE codes, respectively, used in this work. We gratefully acknowledge helpful discussions with C. Mader and C. Volant concerning this work. At GANIL, we appreciate the assistance of the operations and health physics staff who made these measurements possible. This work was supported in part by the U.S. Department of Energy under Grant No. DE-FG06-88ER40402 and the Swedish Natural Sciences Research Council.

[1] E.C. Pollacco *et al.*, Phys. Lett. **146B**, 29 (1984).
[2] M. Conjeaud *et al.*, Phys. Lett. **159B**, 244 (1985).
[3] M. Mostefoi *et al.*, J. Phys., Colloq. **C4**, Supplement **8**, 361 (1986).
[4] D.X. Jiang *et al.*, Nucl. Phys. **A503**, 560 (1989).
[5] J. Galin *et al.*, *Nuclear Dynamics and Nuclear Disassembly,* edited by J.B. Natowitz (World Scientific, Singapore, 1989), pp. 320–326.
[6] H. Delagrange, C. Gregoire, F. Scheuter, and Y. Abe, Z. Phys. A **323**, 437 (1986).
[7] J.P. Lestone, Phys. Rev. Lett. **70**, 2245 (1993).
[8] E.-M. Eckert *et al.*, Phys. Rev. Lett. **64**, 2483 (1990).
[9] E. Mordhurst, M. Strecker, H. Frobeen, M. Gasthuber, W. Scobel, B. Gebauer, D. Hilscher, M. Lehmann, H. Rossner, and Th. Wilpert, Phys. Rev. C **43**, 716 (1991).
[10] D. Utley *et al.*, Phys. Rev. C **49**, R1737 (1994)
[11] E. Vieut *et al.*, Nouvelles du GANIL **46**, 3 (1993); M.F. Rivet *et al.*, Report No. IPNO-DRE-93-12, 1993 (unpublished).
[12] E.C. Pollacco *et al.*, Report No. DAPNIA/SPhN 94 02, February, 1994 (unpublished).
[13] K. Aleklett *et al.*, Nucl. Phys. **A499**, 591 (1989).
[14] F. Hubert, R. Bimbot, and H. Gauvin, At. Data Nucl. Data Tables **46**, 1 (1990).
[15] W. Loveland, K. Aleklett, J.O. Liljenzin, and G.T. Seaborg, J. Radioanal. Nucl. Chem. **160**, 181 (1992).
[16] K. Aleklett, J.O. Liljenzin, W. Loveland, and L. Sihver, Nuclear Physics at GANIL (1989-1991), pp. 114–117 and unpublished data from that experiment.
[17] E. Duek, L. Kowalski, and J.M. Alexander, Comput. Phys. Commun. **34**, 395 (1985).
[18] J.M. Alexander, in *Nuclear Chemistry,* edited by L. Yaffe (Academic, New York, 1968), Vol. I, p. 273.
[19] P.L. McGaughey, W. Loveland, D.J. Morrissey, K. Alek-

lett, and G.T. Seaborg, Phys. Rev. C **31**, 896 (1985).
[20] S. Kox *et al.*, Phys. Rev. C **35**, 1678 (1987).
[21] V.E. Viola, B.B. Back, K.L. Wolf, T.C. Awes, C.K. Gelbke, and H. Breuer, Phys. Rev. C **26**, 178 (1982).
[22] S. Leray, J. Phys. C **4**, 275 (1986).
[23] D.J. Morrissey, W. Loveland, M. de Saint-Simon, and G.T. Seaborg, Phys. Rev. C **21**, 1983 (1980).
[24] B.V. Jacak, W. Loveland, D.J. Morrissey, P.L. McGaughey, and G.T. Seaborg, Can. J. Chem. **61**, 701 (1983).
[25] Y.W. Yu, Phys. Rev. C **22**, 933 (1980).
[26] M. de Saint-Simon, S. Haan. G. Audi, A. Coe, M. Epherre, P. Guimbal, A.C. Mueller, C. Thibault, and F. Touchard, Phys. Rev. C **26**, 2447 (1982).
[27] A. Warwick *et al.*, Phys. Rev. Lett. **48**, 1719 (1982).
[28] W.W. Wilcke, J.R. Birkelund, H.J. Wollersheim, A.D. Hoover, J.R. Huizenga, W.U. Schroder, and L.E. Tubbs, At. Data Nucl. Data Tables **25**, 391 (1980).
[29] W. Loveland, Z. Xu, C. Casey, K. Aleklett, J.O. Liljenzin, D. Lee, and G.T. Seaborg, Phys. Rev. C **38**, 2094 (1988).
[30] M.J. Tobin and P.J. Karol, Nucl. Instrum. Methods A **270**, 511 (1988).
[31] V.P. Crespo, J.M. Alexander, and E. Hyde, Phys. Rev. **131**, 1765 (1963).
[32] J.P. Whitfield and N.T. Porile, Nucl. Phys. **A550**, 553 (1992).
[33] H.M. Blann, Phys. Rev. C **23**, 205 (1981).
[34] W. Bauer, Phys. Rev. C **40**, 715 (1989).
[35] A. Gavron, Phys. Rev. C **21**, 230 (1980).
[36] Th. Blaich, M. Begemann-Blaich, M.M. Fowler, J.B. Wilhelmy, H.C. Britt, D.J. Fields, L.F. Hansen, M.N. Namboodiri, T.C. Sangster, and Z. Fraenkel, Phys. Rev. C **45**, 689 (1992).
[37] Y. Yariv and Z. Fraenkel, Phys. Rev. C **20**, 2227 (1979); **24**, 488 (1981).
[38] J. Toke and W.J. Swiatecki, Nucl. Phys. **A372**, 141 (1981).
[39] W. Reisdorf *et al.*, Nucl. Phys. **A444**, 154 (1985).
[40] D.J. Morrissey, L.F. Oliveira, J.D. Rasmussen, G.T. Seaborg, Y. Yariv, and Z. Fraenkel, Phys. Rev. Lett. **43**, 1139 (1979).
[41] J. Galin *et al.*, in *Nuclear Dynamics and Nuclear Disassembly* [5], pp. 320–336.